Quasi-reversible Faradaic Depolarization Processes in the Electrokinetics of the Metal/Solution Interface

Jérôme F. L. Duval,*,†,‡ Jacques Buffle,† and Herman P. van Leeuwen†,‡

CABE (Analytical and Biophysical Environmental Chemistry), University of Geneva, Sciences II, 30 Quai E. Ansermet, Switzerland, and Department of Physical Chemistry and Colloid Science, Dreijenplein 6, 6703 HB Wageningen, The Netherlands

Received: October 4, 2005; In Final Form: January 26, 2006

Bipolar faradaic depolarization of the metal/solution interface is quantitatively analyzed for the case where the solution is subject to lateral flow and contains a quasi-reversible redox couple. Transversal convective diffusion of the electroactive species and a position-dependent degree of reversibility of the interfacial electron-transfer (e.t.) reaction are among the primary features that govern depolarization. The spatial distributions of species concentrations and electric potential are numerically simulated. The system is characterized by nonlinear coupling between the transport (diffusion and flow) and the electric potential distribution under conditions of finite local currents. The resulting picture is that the reversibility of the e.t. reaction varies with position on the surface, with the highest reversibility downstream. This, in itself, generally leads to strongly asymmetric profiles of the faradaic current density along the surface. The impact on the electrokinetic properties of the interface is huge. For example, the steady-state streaming potential is depressed by the contribution from the bipolar faradaic process to the back current to an extent that varies from insignificant to complete, depending on the e.t. rate constant and concentrations of the electroactive species.

1. Introduction

In recent work,[1] it has been shown that bipolar faradaic depolarization may dramatically impact the electrokinetic features of the interface between a conductor and an electrolyte solution. In the setting of a planar metallic surface and lateral flow of the adjacent electrolyte solution, as applicable in slit cells for streaming potential measurements,[2−4] the effective potential that drives electron-transfer (e.t.) reactions varies with position. Furthermore, the conditions for transport of the electroactive species are nonuniform. At the leading edge (upstream), where fresh solution continually enters the cell, concentration polarization is barely significant. Hence, any electrochemical reaction involving transport of participating species in solution will be primarily limited by the rate of the interfacial e.t. reaction. Further downstream along the surface, concentration polarization becomes more and more significant. As a consequence, one may expect to encounter a transition from irreversible to more reversible behavior, while passing from one end of the surface to the other. Existing theory already covers some inherent features of the bipolar system, including the nonlinear electric field[5] and the combination of a nonlinear field with the flow of solution.[1] These treatments were confined to the limiting cases of totally irreversible or totally reversible e.t. reactions. One has to realize, however, that a gradual change of reversibility with position along the surface is an intrinsic feature of a system with the flow of electrolyte along a conducting surface. Thus, it is timely to extend the theoretical analysis to bipolar faradaic processes with reversibilities that vary with position as a consequence of concentration polarization.

We shall address the most general case with a redox couple that is irreversible at the entrance side of the surface and reversible at the other side. The bipolar nature of the faradaic processes requires that the overall anodic and cathodic currents are the same. This translates to equalities of the integrals over local positive and negative faradaic current densities, as related to the local transversal metal/solution potential difference according to the rigorous current−potential relationship for electrodic processes.[6] It is known already that, even for systems that are supposed to be completely reversible, the concentration profiles for the electroactive species in solution are strongly dependent on position and asymmetrically distributed along the surface. Thus, it may be expected that invoking finite rates of e.t., and corresponding variation of reversibility with position, will compound the complex asymmetry of the concentration and potential profiles along the surface.

With the above in mind, we shall here (i) analyze the essential features of bipolar faradaic depolarization on the basis of the general current−potential relation for e.t. reactions, incorporating both mass transport, as limited by convective diffusion, and finite e.t. rates, and (ii) outline the spatial distributions of the electric potential perpendicular to and along the surface, and the consequences for the electrokinetics of the interface, taking the streaming potential as a representative.

2. Formulation of the Problem

2.1. Geometrical Definition. As before,[1,5] we consider the geometrical situation of a slit cell with two planar, parallel, and identical conducting surfaces, as depicted in Figure 1. This particular type of setting is the common one in electrokinetic studies of the solid/solution interface.[2−4] The basic features

* To whom correspondence should be addressed. Current address: Laboratory for Environmental Sciences and Mineralurgy, UMR 7569 CNRS-INPL, Centre de Recherche François Fiessinger, 15 avenue du Charmois, B.P. 40, 54501 Vandoeuvre-lès-Nancy cedex, France.

† University of Geneva.

‡ Department of Physical Chemistry and Colloid Science.

10.1021/jp055650+ CCC: $33.50 © 2006 American Chemical Society
Published on Web 02/23/2006

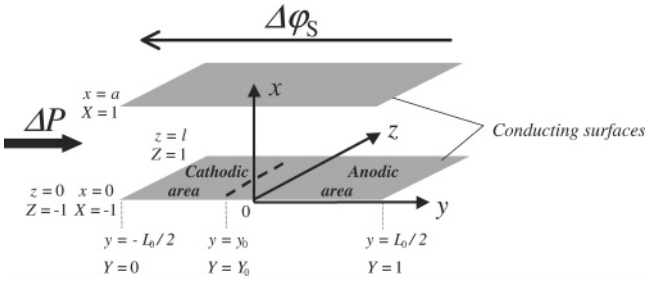

Figure 1. Schematic representation of the planar slit and outline of the notations.

included in the theory of section 2.3 may easily be applied, providing some straightforward modifications regarding the number and magnitude of the kinetic parameters, to other situations of practical importance, that is, when the channel consists of one conducting and one dielectric surface or even two conducting surfaces of different nature. At either side of the slit compartment, that is, for $y = \pm L_o/2$, there is an open connection with a reservoir of electrolyte solution. A pressure gradient, ΔP, is applied long the *y*-axis to cause a proportional flow of electrolyte solution; the sign of ΔP is chosen such that the flow is toward larger *y*, that is, from left to right in the diagram of Figure 1. For convenience in the description of the bipolar phenomena, the Cartesian coordinate system *x*,*y*,*z* is defined such that $y = 0$ corresponds with the cross-section in the center of the slit cell, as shown in Figure 1. The distance between the two metallic surfaces is *a*, their length L_o, and their width *l*. The electrolyte solution has a conductivity K^L, a relative dielectric permittivity ϵ_r, and a dynamic viscosity η; it contains a redox couple, denoted as Ox/R, which exhibits electroactive behavior for the particular surfaces considered. This means that we are envisaging the interfacial electron-transfer reaction

$$\mathrm{Ox} + n\mathrm{e}^- \rightleftarrows \mathrm{R} \tag{1}$$

where *n* is the number of electrons involved. In some of the computations, an electric field is applied across the solution along the *y*-axis. The corresponding potential difference between the two ends of the cell compartment is denoted as $\Delta\varphi_s$. With a finite $\Delta\varphi_s$, the two surfaces may exhibit the behavior of bipolar electrodes. We arbitrarily locate the *positive* side of the electric field in the *left upstream* part of the cell, where consequently the *cathodic* reduction reaction is provoked.

In the following, it will be convenient to use the dimensionless spatial variables *X*,*Y*,*Z* defined as

$$X = \frac{2}{a}\left(x - \frac{a}{2}\right)$$

$$Y = \frac{1}{L_0}\left(y + \frac{L_0}{2}\right)$$

$$Z = \frac{2}{l}\left(z - \frac{l}{2}\right) \tag{2}$$

We shall assume that the supporting electrolyte in solution is in sufficient excess over the redox components so that conductive transport of the electroactive species can be neglected. The e.t. reaction (eq 1) is rate-limited by the convective diffusion to/from the surfaces of the electroactive species Ox and R and by the very electron-transfer step at the interface. To derive the overall bipolar current, denoted I_f, analysis of the hydrodynamic situation is first required. Then, the set of equations for the calculation of the concentration profiles of Ox/R and the spatial distributions of potential and local faradaic current density can be formulated.

2.2. Velocity Profile. The flow direction is parallel to the surfaces (*y*-direction) and the steady-state velocity profile is represented by $v_Y(X,Z)$, as formulated by the pertaining Navier−Stokes equation

$$\frac{\partial^2 v_Y(X,Z)}{\partial X^2} + \phi^2 \frac{\partial^2 v_Y(X,Z)}{\partial Z^2} = -\frac{a^2}{4\eta}\frac{\Delta P}{L_0} \tag{3}$$

with $\phi = a/l$. It has been shown that, in the relevant pressure domain, hydrodynamic steady-state conditions apply and the flow is laminar.[1] At the walls of the cell, we have the boundary conditions

$$v_Y(X = \pm 1, Z) = v_Y(X, Z = \pm 1) = 0 \tag{4}$$

The general solution $v_Y(X,Z)$ of eqs 3−4 is given by[7]

$$v_Y(X,Z) = v^0\left\{(1 - X^2) + \frac{32}{\pi^3}\sum_{m=1}^{\infty}\frac{(-1)^m}{(2m-1)^3}\cos\left[(2m-1)\frac{\pi}{2}X\right] \times \cosh\left[(2m-1)\frac{\pi}{2}\frac{Z}{\phi}\right]\mathrm{sech}\left[(2m-1)\frac{\pi}{2}\frac{1}{\phi}\right]\right\} \tag{5}$$

where v^0 is the characteristic velocity

$$v^0 = \frac{a^2}{8\eta}\frac{\Delta P}{L_0} \tag{6}$$

As explained before,[1] for the type of thin-layer cell discussed here (Figure 1), it suffices to consider the Poiseuille profile (first term within brackets in eq 5) for an infinitely wide channel ($\phi \rightarrow 0$).

2.3. Coupling between Reactant Transport and Electrostatics. The concentration profiles of the electroactive species, denoted as $c_{Ox}(X,Y)$ and $c_R(X,Y)$ for the Ox and R species, respectively, are determined by the electric field, the electrode kinetics, and the characteristics of the diffusive and convective mass-transport processes. Symmetry of the problem with respect to the *Z*-dimension follows from the previous discussion and justifies that c_{Ox} and c_R are not functions of *Z*, that is, edge effects at $Z = \pm 1$ are negligible. Transient effects need not be considered as the time scale of measurement, τ_M, is much larger than $\delta^2/\pi D$, the time constant for building-up a diffusion layer of thickness δ by species with diffusion coefficient *D*. Consequently, the local faradaic currents along the surfaces are limited by diffusion of the species in the *X*-direction and by convection in the *Y*-direction. By way of example, we examine the cathodic reaction and the profile for $c_{Ox}(X,Y)$. For the sake of convenience, we define the dimensionless concentration difference

$$C_{Ox}(X,Y) = \frac{c_{Ox}(X,Y) - c^*_{Ox}}{c^*_{Ox}} \tag{7}$$

where c^*_{Ox} is the bulk concentration of species Ox, that is, the initial homogeneous concentration of Ox. Under the conditions outlined above, the Nernst−Planck equation reduces to that for convective diffusion. For the Ox species, it reads

$$v^0(1-X^2)\frac{\partial C_{Ox}(X,Y)}{\partial Y}=\frac{4D_{Ox}L_0}{a^2}\frac{\partial^2 C_{Ox}(X,Y)}{\partial X^2} \quad (8)$$

where D_{Ox} is the diffusion coefficient of Ox. Resolution of eq 8 requires two boundary conditions with respect to X and one related to the Y-direction. The latter is simply written

$$C_{Ox}(X,Y=0)=0 \quad (9)$$

which expresses that, at the left side of the channel, electroactive species are injected from the reservoir with bulk concentrations c^*_{Ox} and c^*_R. The two remaining conditions (at $X=\pm 1$) derive from the coupling of the mass balance for Ox and R and the expression for the rate of the interfacial electron-transfer reaction. The mass balance condition is simply written

$$j(Y)=\frac{2nFD_{Ox}}{a}\frac{\partial c_{Ox}(X,Y)}{\partial X}|_{X=1}=\frac{-2nFD_R}{a}\frac{\partial c_R(X,Y)}{\partial X}|_{X=1} \quad (10)$$

and similar expressions hold at $X=-1$. The quantity $j(Y)$ is the faradaic current density at the position Y, D_R the diffusion coefficient of R, and F the Faraday number. If we assume that the diffusion coefficients for Ox and R are equal ($D=D_{Ox}=D_R$) and that the total concentrations of Ox and R at the boundaries remain constant (protonation reactions of the redox species at the surfaces and/or in the bulk or other modifications of c^*_{Ox} and c^*_R are not considered here), then eq 10 simplifies into

$$c_{Ox}(X=\pm 1,Y)+c_R(X=\pm 1,Y)=c^*_{Ox}+c^*_R \quad (11)$$

The current density $j(Y)$ is further given by the general current−potential relationship for electrodic processes[6]

$$j(Y)=nFk_o\{-c_{Ox}(X=\pm 1,Y)\exp[nf\alpha(V(Y)-V^o)]+c_R(X=\pm 1,Y)\exp[-nf(1-\alpha)(V(Y)-V^o)]\} \quad (12)$$

where reduction currents are counted negative. k_o is the rate constant and α ($0\le\alpha\le 1$) is the transfer coefficient. It is mentioned that, within the scope of the current analysis, the dependence of k_o on the local double-layer structure is, for the sake of simplicity, not considered so that k_o refers to the standard (or intrinsic) rate constant of reaction 1. In the situations where k_o values depend on the double-layer composition, like in ref 8, k_o should be replaced in eq 12 by the true rate constant that contains the appropriate Boltzmann factor necessary for expressing the actual concentrations of Ox and R at the surface (Frumkin corrections[9]). In eq 12, $V(Y)$ denotes the potential of the solution at the position Y with respect to the (equipotential) metallic surfaces, V^o is minus the standard potential of the redox couple Ox/R, and f is the constant

$$f=\frac{F}{RT} \quad (13)$$

with T the absolute temperature and R the gas constant. Combining eqs 11−12 yields the searched boundaries at $X=\pm 1$ associated with eq 8, that is, for the surface concentration of the Ox species

$$C_{Ox}(X=\pm 1,Y)=Q(Y)-\gamma j(Y)G(Y) \quad (14)$$

with

$$\gamma=1/k_oFc^*_{Ox} \quad (15)$$

$$Q(Y)=\frac{c^*_{Ox}+c^*_R}{c^*_{Ox}}\frac{\exp\{-nf(V(Y)-V^o)\}}{1+\exp\{-nf(V(Y)-V^o)\}}-1 \quad (16)$$

and

$$G(Y)=\frac{\exp\{-n\alpha f(V(Y)-V^o)\}}{1+\exp\{-nf(V(Y)-V^o)\}} \quad (17)$$

In the limiting case of reversible faradaic reactions, the kinetics of the e.t. reaction 1 is very fast ($k_o\to\infty$) so that eq 14 reduces to

$$C_{Ox}(X=\pm 1,Y)|_{ko\to\infty}\to Q(Y) \quad (18)$$

The limit (eq 18) expresses the Nernstian equilibrium between the surface concentrations of the electroactive species with the potential $V(Y)$, as considered in ref 1 for the examination of fully reversible bipolar faradaic depolarization processes. The second term in the right-hand side of eq 14 depends on the kinetic parameters k_o and α and thus accounts for the impact of the finite rate of the e.t. reaction on the current density.

To compute the profiles of Ox, the potential distribution $V(Y)$ must be known. There is a nonlinear intrinsic coupling between $C_{Ox}(X,Y)$ and $V(Y)$, as subsumed in eqs 14−17. The equation defining $V(Y)$ is provided by the electroneutrality condition written for every $X-Z$ slice along the surfaces. In the geometry considered here, the resulting Poisson equation for finite currents is written

$$\frac{aK^L}{L_0^2}\frac{d^2V(Y)}{dY^2}+2j(Y)=0 \quad (19)$$

The derivation of eq 19 is given in detail in ref 5. Here, we shall only recall the approximations made and the conditions for which these are valid, that is:

(i) The potential distribution related to the double-layer formation at the two interfaces metal/solution is neglected, which is justified provided that the Debye length κ^{-1} is much smaller than the position-dependent diffusion layer thickness $\delta(Y)$ and the gap a between the two parallel surfaces.

(ii) The electric field across the solution is assumed to be time independent, with the transport processes under steady-state conditions.

(iii) The chemical composition of the solution remains essentially constant during the experiment (constant K^L), which is true in the presence of an indifferent electrolyte in sufficient excess over the electroactive species (this also ensures the validity of $\kappa^{-1}\ll\delta(Y)$).

The two boundary conditions related to eq 19 are provided by the potential balance in solution and the condition of no-charge accumulation in the conducting substrates, that is[1]

$$V(Y=0)-V(Y=1)=\Delta\varphi_s \quad (20)$$

and

$$\int_0^1 j(Y)\,dY=0 \quad (21)$$

respectively. Through the use of eq 19, boundary (21) may be written as $dV(Y)/dY|_{Y=0}=dV(Y)/dY|_{Y=1}$. The determination of $C_{Ox}(X,Y)$, $j(Y)$, and $V(Y)$ requires numerical resolution of the system of coupled eqs 8, 9, 12, 14−17, and 19−21. Details of the computational procedure are reported in the Appendix. Once $j(Y)$ is known for given $\Delta\varphi_S$ and ΔP values, the corresponding

overall bipolar current I_f is obtained by integration of the local current density $j(Y)$

$$I_f = -2lL_0 \int_0^{Y_0} j(Y)\,dY = 2lL_0 \int_{Y_0}^{1} j(Y)\,dY \qquad (22)$$

where Y_0 is the position for which $j(Y = Y_0) = 0$. The potential difference between the solution and metallic phases at that position, $V(Y = Y_0)$, corresponds to the equilibrium potential denoted as V^*. Combining eqs 19 and 22, I_f may also be expressed as a function of the electric field at the position $Y = Y_0$ compared with the front or back edge of the cell ($Y = 0$ or $Y = 1$)

$$I_f = \frac{alK^L}{L_0}\left(\left.\frac{dV(Y)}{dY}\right|_{Y=Y_0} - \left.\frac{dV(Y)}{dY}\right|_{Y=0}\right) = \frac{alK^L}{L_0}\left(\left.\frac{dV(Y)}{dY}\right|_{Y=Y_0} - \left.\frac{dV(Y)}{dY}\right|_{Y=1}\right) \qquad (23)$$

3. Results and Discussion

3.1. Impact of the Rate Constant k_o on the Characteristics of the Bipolar Process. 3.1.1. Bipolar Current I_f. The dependence of the bipolar current I_f on the e.t. rate constant k_o is shown in Figure 2A for various values of the applied pressure ΔP and constant applied field $\Delta\varphi_S$. The values chosen for k_o reflect that e.t. rate constants may range over more than 10 orders of magnitude.[10] Upon the increase of k_o, I_f gradually increases before leveling off. In the limiting regime where concentration polarization is absent or insignificant, that is, for sufficiently low values of k_o, the sluggish kinetics of the e.t. reaction 1 solely determines the rate of the bipolar faradaic processes. I_f then is essentially independent of the mass-transport conditions of the electroactive species and hence independent of the applied pressure gradient ΔP (*irreversible* limit). Within this range of values for k_o, the bipolar current I_f approaches that calculated on the basis of the theory developed in ref 5 for fully irreversible bipolar faradaic reactions (dashed line in Figure 2A). In passing, we note that the later (analytical) theory applies for e.t. reactions so irreversible that in the cathodic region the anodic current component can be neglected and vice versa. The numerical evaluation of the irreversible case reported in Figure 2A was performed after relaxing this condition as necessary when passing to higher k_o values. For sufficiently large k_o, that is, for fast interfacial e.t., I_f reaches a plateau, the value of which increases with increasing ΔP. The rate of the bipolar process is then solely determined by the convective diffusion (mass transport) of Ox and R to/from the surfaces (*reversible limit*). We verified that the corresponding currents I_f are in agreement with those obtained from the theory for fully reversible bipolar processes reported in ref 1. In particular, within the conditions of Figure 2A, for $\Delta P < 0.05$ kPa, $I_f(k_o \to \infty)$ identifies to the *diffusive limiting current*, I_f^l, corresponding to maximum transport rate of Ox (respectively, R). Within the window of the two k_o values defined by the irreversible and reversible limits discussed above, the bipolar current is simultaneously governed by the electrode kinetics *and* convective diffusion of the electroactive species, the *quasi-reversible* case. Then, I_f increases with increasing ΔP for a given k_o as a result of the local decrease of the diffusion layer for every position Y along the bipolar electrodes. Similarly to monopolar faradaic reactions for which the appearance of kinetic effects depend on the time window of the experiment, the degree of reversibility for a bipolar process is clearly a function of the pressure gradient (which mediates the velocity profile, eqs 5−6) applied across the cell.

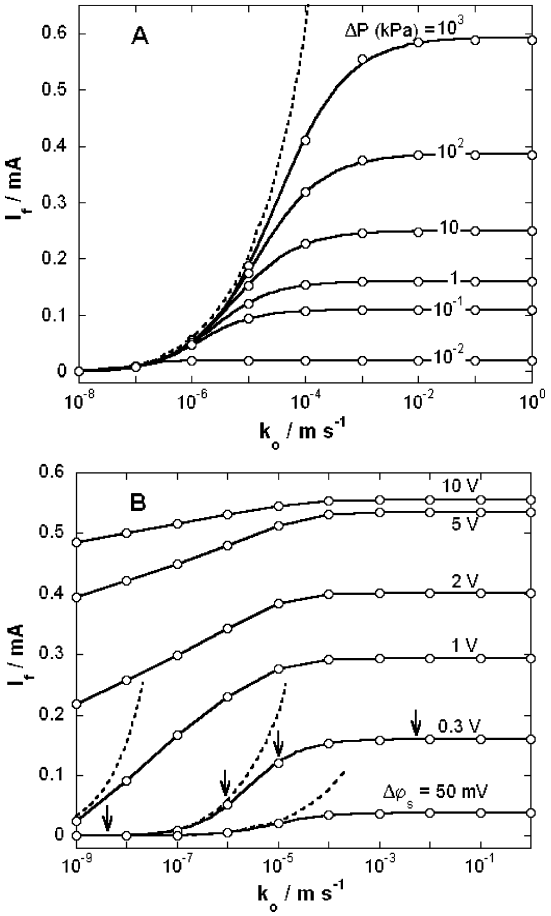

Figure 2. Bipolar current (points) as a function of the electron-transfer rate constant k_o at different applied pressures ΔP (A) and electric fields $\Delta\varphi_s$ (B) (indicated). The dashed lines represent the bipolar current as computed for irreversible—that is, kinetically controlled—anodic and cathodic reactions (absence of concentration polarization, i.e., $c_{Ox} = c_{Ox}^*$ and $c_R = c_R^*$). Model parameters: $a = 0.2$ mm, $L_0 = 7.6$ cm, $l = 2.6$ cm, $D = 10^{-9}$ m^2 s^{-1}, $V^0 = -233$ mV, $K^L = 1\ \Omega^{-1}$ m^{-1}, $\alpha = 0.5$, $c_{Ox}^* = c_R^* = 0.1$ mM, and $\Delta\varphi_s = 0.3$ V (A) and $\Delta P = 1$ kPa (B). Plain lines are only a guide to the eye. The arrows in panel B point out the bipolar currents associated with the spatial distributions for the Ox species given in Figure 3.

When ΔP is increased, I_f approaches the irreversible limit over a broad range of k_o values. This is so because, upon the increase of lateral convection, the extent of concentration polarization is diminished. As a result, the very electron-transfer step at the interface plays an increasingly leading role in determining the rate of reaction 1.

Figure 2B illustrates the dependence of I_f on k_o for various applied fields $\Delta\varphi_S$ and constant pressure drop ΔP. For $\Delta\varphi_S = 0$ (not shown), the local overpotential $V(Y) - V^*$ (which governs the activation energy for the e.t. at the positions $(X = \pm 1, Y)$) is zero everywhere along the surface, so that the surface concentrations equal their bulk values and $I_f = 0$ irrespectively of the kinetic rate constant k_o. For a finite $\Delta\varphi_S$, the irreversible and reversible electrodic regimes can be identified in a way similar to that adopted for Figure 2A. In particular, for the pressure condition of Figure 2B, the bipolar current corresponding to fully reversible functioning of the faradaic processes reaches the diffusive limiting current I_f^l for $\Delta\varphi_S \geq 10$ V. For a given intermediate value of k_o (*quasi-reversible* behavior of the electrodes), I_f increases with $\Delta\varphi_S$ because the local overpotentials $V(Y) - V^*$ and the resulting rates of the local mass transfer for Ox and R increase in magnitude (increase of the interfacial

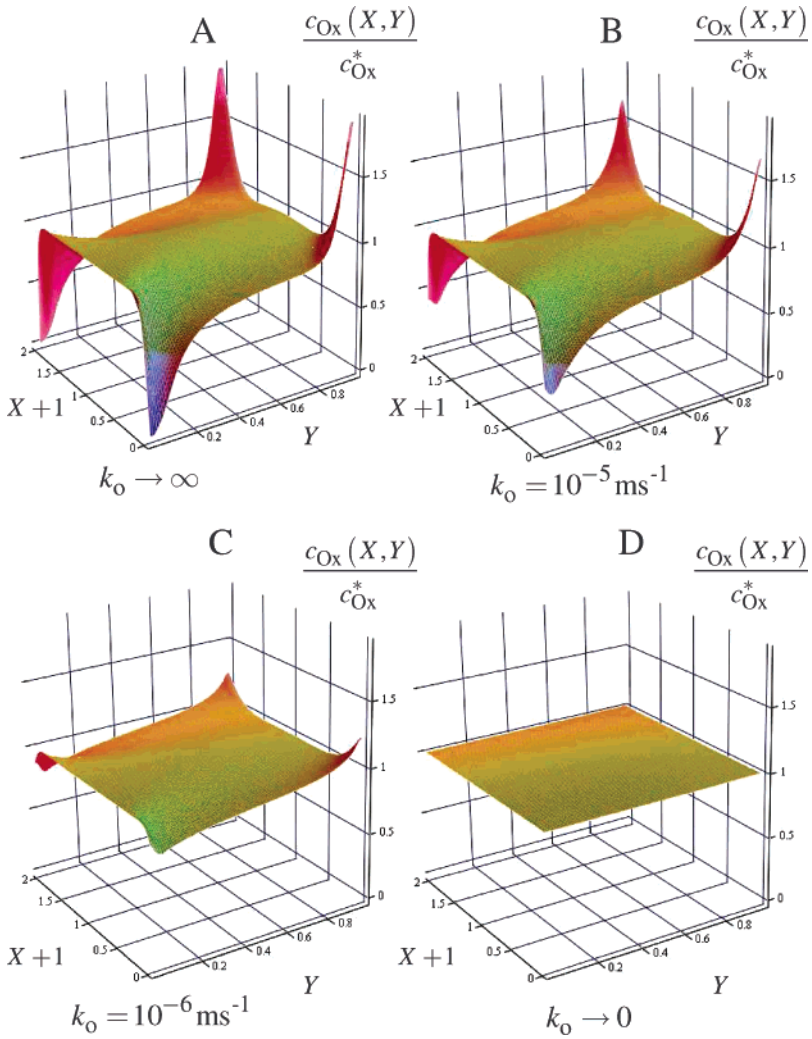

Figure 3. Concentration profiles of the oxidized form of the redox couple at varied electron-transfer rate constants k_o (indicated): $\Delta P = 1$ kPa and $\Delta\varphi_s = 0.3$ V. Other parameters are the same as those in Figure 2. The profiles at the injection position $Y = 0$ (left extremity of the cell) are not drawn ($c_{Ox} = c^*_{Ox}$).

concentration gradients). I_f then gradually approaches the reversible limit. As a result, upon the increase of $\Delta\varphi_S$, the window of rate constants associated with the irreversible limit is progressively displaced to lower values of k_o, as expected from classical electrodic theory for monopolar processes.[6]

3.1.2. Concentration Profiles. The spatial distributions of the Ox species in the X and Y directions are shown in Figure 3 for various values of k_o and $\Delta\varphi_S = 0.3$ V/$\Delta P = 1$ kPa. The corresponding bipolar currents may be read from the pertaining data (marked by arrows) depicted in Figure 2B. For $k_o \to \infty$ (panel A), the profile $c_{Ox}(X,Y)$ is in line with that obtained from the theory for reversible bipolar depolarization as extensively discussed in ref 1. The surface concentration $c_{Ox}(X = \pm 1,Y)$ progressively increases from left to right as a result of the passage from reduction to oxidation reaction. Focusing our attention on the cathodic area ($0 < Y < Y_o$ with $Y_o \approx 0.65$ under the conditions of Figure 3A, see Figure 5), the surface concentration gradient is maximum at the injection point of the cell and becomes less significant when moving toward Y_o. This is a direct consequence of the spatial dependence of the diffusion layer δ on position Y ($\partial\delta/\partial Y > 0$).[1,11] With decreasing k_o (panels B and C), the finite rate of the e.t. reaction 1 becomes more and more dominant and local surface concentration gradients of Ox and R are diminished. In the limit $k_o \to 0$, $c_{Ox}(X,Y) \to c^*_{Ox}$ everywhere within the thin-layer channel ($I_f \to 0$). The features discussed above are further illustrated in Figure 4 where cross-sections of the profiles represented in Figure 3 are given for various lateral positions Y. The trivial case $k_o \to 0$ does not need any further comment. It is clear that for sufficiently small a and/or sufficiently large ΔP, the characteristic diffusion length δ increases from $Y = 0$ to $Y = Y_o$ (panels A−C, cathodic area), to reach at some point the value $a/2$ where subsequent depletion of the reactant species (plus accumulation of product) occurs. The more sluggish the kinetics of the e.t. (the lower k_o), the less determining the convective diffusion process becomes and the lower the extent of this depletion. Expressed differently, the quantity C_{Ox} defined in eq 7 is reduced for every X upon the increase of k_o. Closer inspection of the profiles reveals that for a given k_o the deviations of the surface concentrations c_{Ox}-$(X = \pm 1,0 < Y < Y_o)$ from those obtained for $k_o \to \infty$ are clearly a function of Y. At the entrance of the cell (upstream), where δ effectively starts from zero, the deviations of $c_{Ox}(X,Y = 0)$ from the bulk value c^*_{Ox} are located in the close vicinity of the channel surfaces ($X = \pm 1$) only. The concentration polarization is thus minimal and the local current density $j(Y = 0)$ is very sensitive to the electrode kinetics, that is, the intrinsic rate constant k_o. More downstream, those deviations span over broader X ranges, the concentration polarization is therefore larger, due to larger δ values (see depletion effects mentioned above), and the e.t. kinetics limits the rate of reaction 1 to a

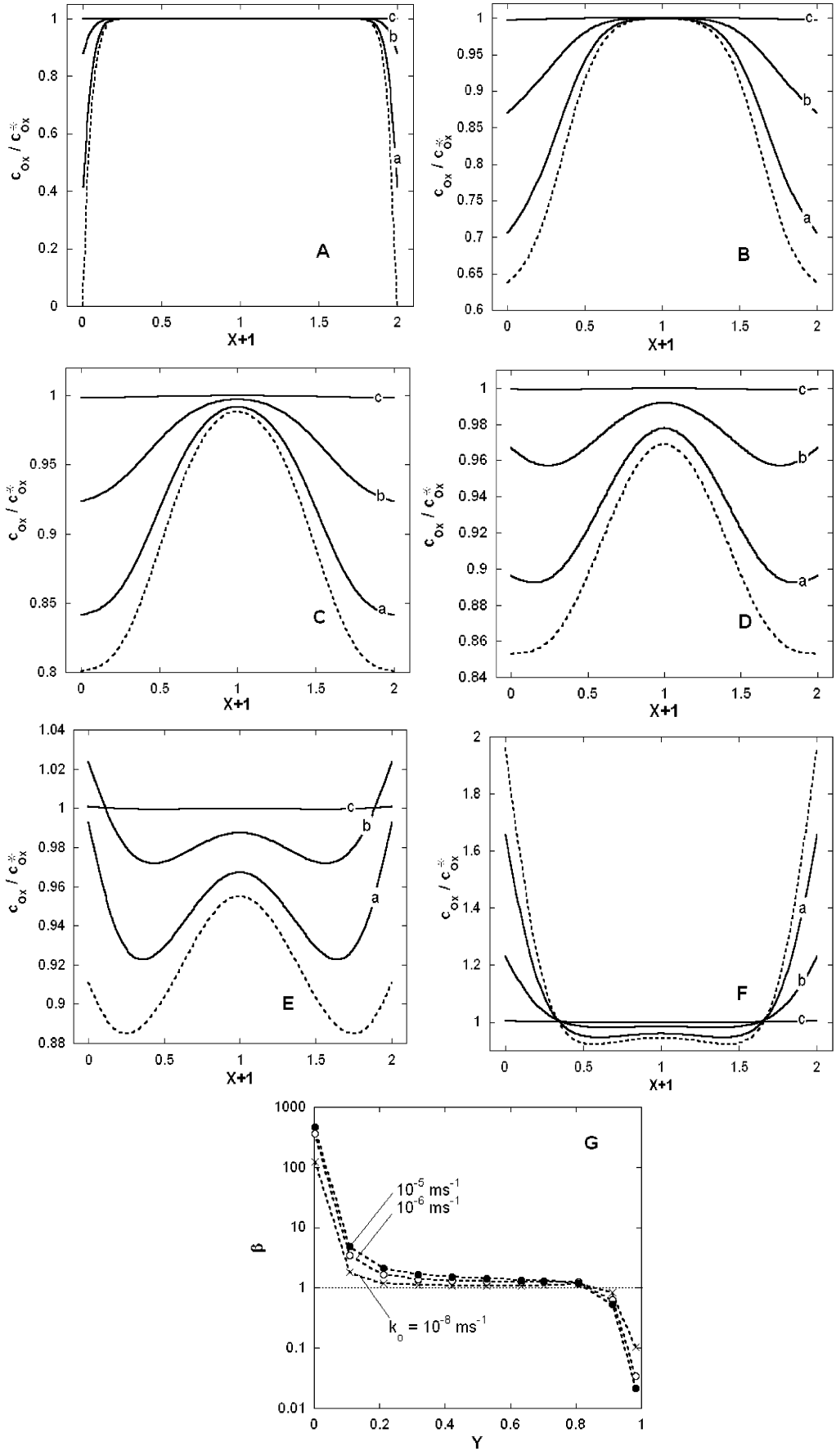

Figure 4. Cross-sections of the concentration profiles c_{Ox}/c^*_{Ox} represented in Figure 3 at the positions $Y = 0.0025$ (A), 0.2125 (B), 0.4225 (C), 0.6325 (D), 0.8075 (E), and 0.9825 (F) for four values of k_o (in m s^{-1}): (dashed curve) $k_o \rightarrow \infty$, (a) $k_o = 10^{-5}$, (b) $k_o = 10^{-6}$, and $k_o = 10^{-8}$ (c). (G) Plot of the ratio $\beta = (c_{Ox}/c_R)_{X=1,ko}/(c_{Ox}/c_R)_{X=1,ko\rightarrow\infty}$ for various k_o (indicated) as a function of the lateral position Y. Other model parameters are the same as those in Figure 3.

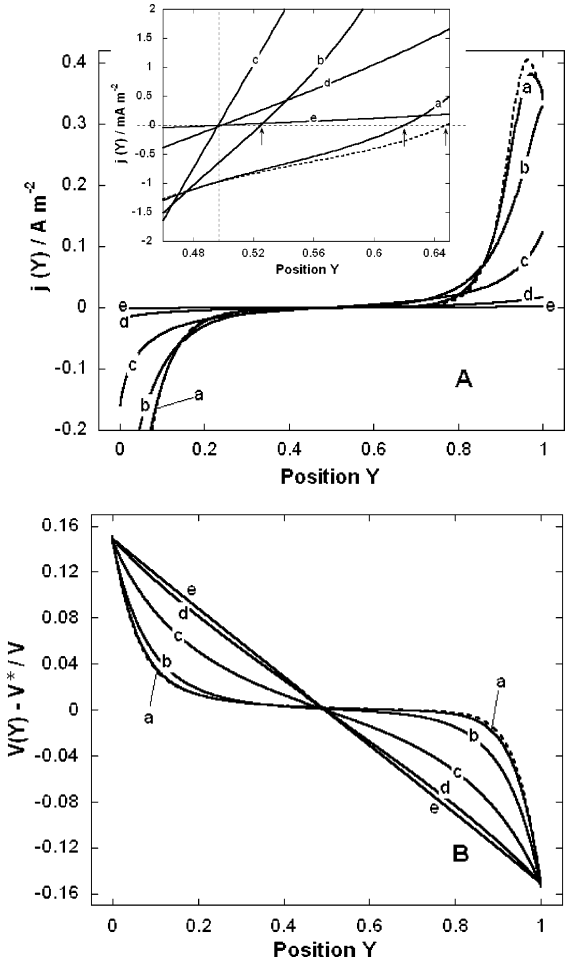

Figure 5. Spatial distributions of the local faradaic current density $j(Y)$ (A) and the local potential $V(Y)$ (B) along the conducting surface at different electron-transfer rate constants k_o: $\Delta P = 1$ kPa and $\Delta\varphi_s = 0.3$ V. Common to panels (A) and (B): $k_o = 10^{-4}$ (curves a), 10^{-5} (curves b), 10^{-6} (curves c), 10^{-7} (curves d), and 10^{-8} (curves e) m s^{-1}. The dashed lines represent the current and potential distributions for a fully reversible bipolar process (electron-transfer rates limited by mass-transport processes). The distributions depicted in curves (b) and (c) correspond to the concentration profiles given in parts B and C of Figure 3 (quasi-reversible bipolar electrodics), whereas the dashed curve (fully reversible case) and curve (e) (fully irreversible case) correspond to parts A and D of Figure 3, respectively. Other model parameters are the same as those in Figure 2. In the inset of Figure 5A, the behavior of $j(Y)$ in the vicinity of $Y = Y_o$ is magnified.

lesser extent. To put it in a nutshell, the degree of reversibility is manifestly a function of the lateral position Y and increases in the direction of the flow. This is further illustrated in Figure 4G where the ratio $\beta = (c_{Ox}/c_R)_{X=1,k_o}/(c_{Ox}/c_R)_{X=1,k_o\to\infty}$ is plotted as a function of the lateral position Y. For $0.1 < Y < 0.9$, β gradually decreases with Y for all k_o values investigated and asymptotically reaches the value 1. At the entrance of the cell ($Y = 0$), for a given k_o, the deviations of β from 1 are about 1 order of magnitude larger than those obtained at the exit of the cell ($Y = 1$). These quantitative elements confirm the increase of the degree of reversibility along the channel wall in the direction of the flow.

Let us now analyze the concentration profiles pertaining to the anodic area of the electrode (panels D−F). As already discussed in ref 1, the presence of the local minima (located at $-1 < X < 0$ and $0 < X < 1$) is due to the oxidation of R at the surfaces and the overshoot of R (as produced in the cathodic area and introduced by the flow for $Y > Y_o$) with respect to the position $X = 0$. At the downstream side of the cell ($Y = 1$) (panel F), the variation of the surface concentration gradient with k_o is in line with the idea that a slower reaction kinetics is accompanied by a decrease of the local current density j, as defined in eq 10 ($\partial\{(dc_{Ox}/dX)_{X=\pm1}\}/\partial k_o > 0$). The dependence of j on k_o for $Y < 1$, as inferred from the surface concentration gradients of panels D and E, does not clearly follow this basic argument since (i) the presence or absence of the local minima is a function of k_o (panel D) and (ii) the variations of j with k_o may be nonmonotonic (panel E). The reason for this peculiar behavior is related to the changes of symmetry for the concentration profiles as induced by the spatially dependent degree of reversibility. These changes compound those mediated by the convective diffusion characteristics of the e.t. reaction. For purely reversible bipolar faradaic processes, the inhomogeneous distribution of δ along the electrodes implies a strong variation of Y_o with ΔP (see ref 1 for further detail). For quasi-reversible e.t., the kinetic limitation comes on top of it.

The two basic features outlined above, that is, the position-dependent degree of reversibility along the bipolar surfaces and the related changes in symmetry for the concentration profiles, are further discussed in the next section where spatial distributions for the current density $j(Y)$ and potential $V(Y)$ are explicitly examined.

3.1.3. Current Density and Potential Profiles. In Figure 5, we give the profiles of $j(Y)$ and $V(Y)$ calculated for various k_o, the other conditions being those adopted in Figures 3 and 4. The anodic and cathodic branches of the 3-D concentration profiles (or of the space-projected voltammograms, see ref 12) depicted in panel A for $k_o \to \infty$ (dashed curve) conform to those obtained for fully reversible processes.[1] In particular, (i) the maximum observed for $Y > Y_o$ originates from the local overshoot of R in the anodic area, which is reflected in the presence of local minima for $c_{Ox}(X,Y)$ (see discussion in section 3.2) and (ii) Y_o is larger than $^1/_2$ (in the case $c^*_{Ox} = c^*_R$) to maintain the requirement of no charge accumulation in the substrate, as expressed by the equality of the current density integrals over the anodic and cathodic areas. For reversible systems, it is recalled that Y_o depends on the magnitude of the applied pressure and on that of the lateral electric field.[1] Upon the decrease of k_o, the aforementioned maximum in current density disappears and the voltammograms flatten with the limit $j(Y) \to 0$ when $k_o \to 0$. By doing so, Y_o is shifted to the left reaching the value of $^1/_2$ when $k_o \to 0$ (inset Figure 5A) and the voltammograms become more antisymmetric around the position Y_o, that is, $j(Y_o + \Delta Y) + j(Y_o - \Delta Y) \xrightarrow[k_o\to0]{} 0$. These symmetry features follow directly from eq 12 with $c_{Ox,R}(X = \pm1,Y) \xrightarrow[k_o\to0]{} c^*_{Ox,R}$, $\alpha = ^1/_2$, and $c^*_{Ox} = c^*_R$ (model parameters chosen for Figure 5). The presence of a position-dependent degree of reversibility along the electrode is evident from Figure 5A when noticing that, for $k_o \to \infty$, the larger current densities are located in the cathodic area (because of the higher diffusion rates), whereas for lower values of k_o, antisymmetry is approached.

In Figure 5B, the computed potential distributions $V(Y) - V^*$, with V^* the equilibrium potential $V(Y = Y_o) = V^*$, are according to expectations. For sufficiently large values of k_o, and a significant bipolar current as compared with its ohmic counterpart, the profiles deviate considerably from linearity. This is an immediate consequence of the intrinsic (nonlinear) coupling between ionic and electronic conduction processes[5] as expressed by the first and second terms in eq 19, respectively. The exponential-type dependence of the current density on the local overpotentials explains that faradaic depolarization is the

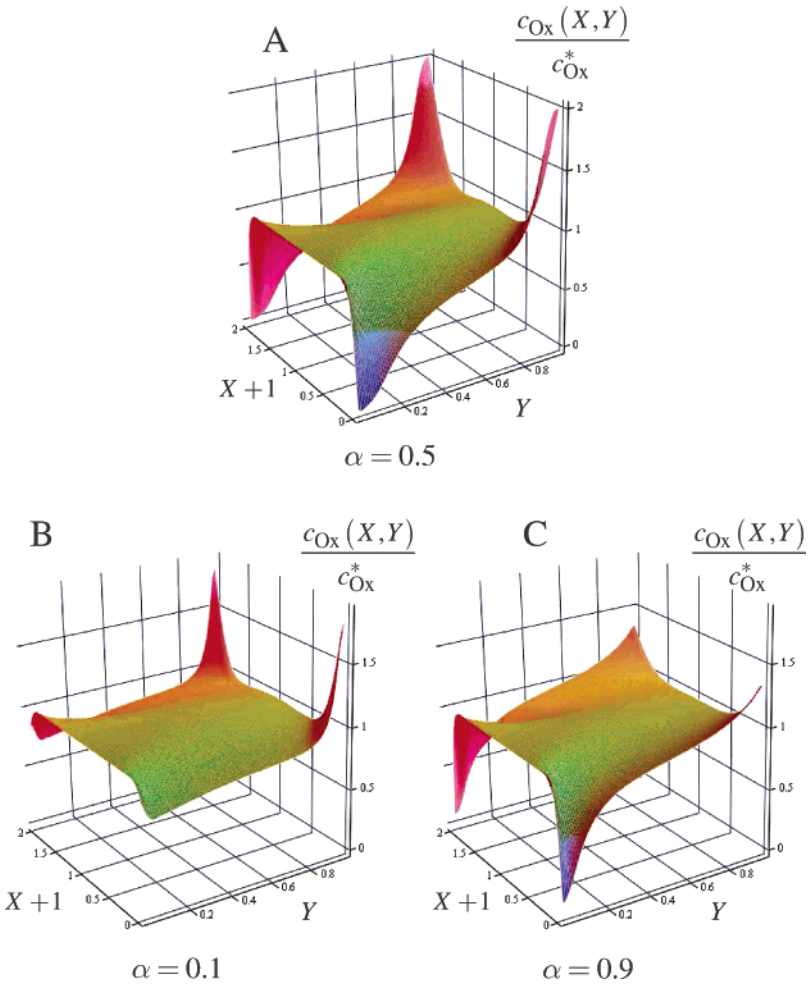

Figure 6. Concentration profiles of the oxidized form of the redox couple at different electron-transfer coefficients α (indicated). Other parameters are the same as those in Figure 2 except $\Delta P = 1$ kPa, $\Delta\varphi_s = 1$ V, and $k_o = 10^{-6}$ m s^{-1}. The profiles at the injection position $Y = 0$ (left extremity of the cell) are not drawn ($c_{Ox} = c^*_{Ox}$).

most important at the inlet and outlet of the thin-layer chamber where the larger electric fields are found.

3.2. Impact of the Coefficient Transfer α on the Characteristics of the Bipolar Process. 3.2.1. Concentration Profiles. Given the influence of the finite rate constant k_o on the bipolar behavior as discussed in section 3.1, we now propose to examine in detail the impact of the other parameter required to model the electrode kinetics, that is, the coefficient transfer α. To start with, concentration profiles pertaining to quasi-reversible functioning of the bipolar electrodes are shown in Figure 6 for various values of α. Whereas for $\alpha = {}^1/_2$ (panel A), the spatial distribution $c_{Ox}(X,Y)$ exhibits a particular symmetry around the position mid-way through the electrode surfaces (see section 3.1), that symmetry is lost for $\alpha < {}^1/_2$ (panel B) and $\alpha > {}^1/_2$ (panel C). To understand this, it is necessary to come back to the physical interpretation commonly assigned to α. Within the framework of the transition-state theory, α is basically an indicator of the symmetry of the energy barrier to the e.t. reaction 1.[13] For a given positive electrode potential where anodic oxidation is supposed to occur, increasing α to values larger than ${}^1/_2$ leads to an increase of the standard free energy associated with the activated complex of which the location is shifted to larger reaction coordinates. As a result, the barrier energy for the oxidation reaction increases and the corresponding net transformation of R to Ox is lowered. This argumentation is in line with the concentration profiles $c_{Ox}(X,Y)$ of parts A and C of Figure 6. In the anodic area (large Y), the local concentration polarizations are significantly reduced upon the increase of α. Similar reasoning applies to the changes in the local concentration polarizations within the cathodic area (small Y) when decreasing α (parts A and B of Figure 6). A closer inspection of the current density and potential profiles corresponding to Figure 6 reveal other interesting features that are discussed in the next section.

3.2.2. Current Density and Potential Profiles. The spatial distributions of the local current density j and overpotentials $V - V^*$ are given in Figure 7 for various values of α. As similar to the analysis of the concentration profiles in section 3.2.1, the cathodic/anodic branch of the voltammograms is significantly affected as a result of the decrease/increase of α below/above 0.5 (parts A and B of Figure 7, respectively). The decrease of the (net) rate of the reduction (oxidation) reaction is roughly speaking reflected in a gradual suppression of the corresponding j. These changes in the profiles j within the cathodic (anodic) area are always accompanied by subtle modulations of j pertaining to the anodic (respectively, cathodic) parts of the electrode. This is so because of the nonlinear coupling between the oxidation and reduction processes as governed by lateral hydrodynamics and the condition of no-charge accumulation in the bipolar electrodic system (eq 21). The former is responsible for the peculiar variations (in position and magnitude) of the anodic peak current with α (Figure 7A), and the latter results in a shift of the position Y_o toward the left part of the electrode when increasing α from 0 to 1. This dependence

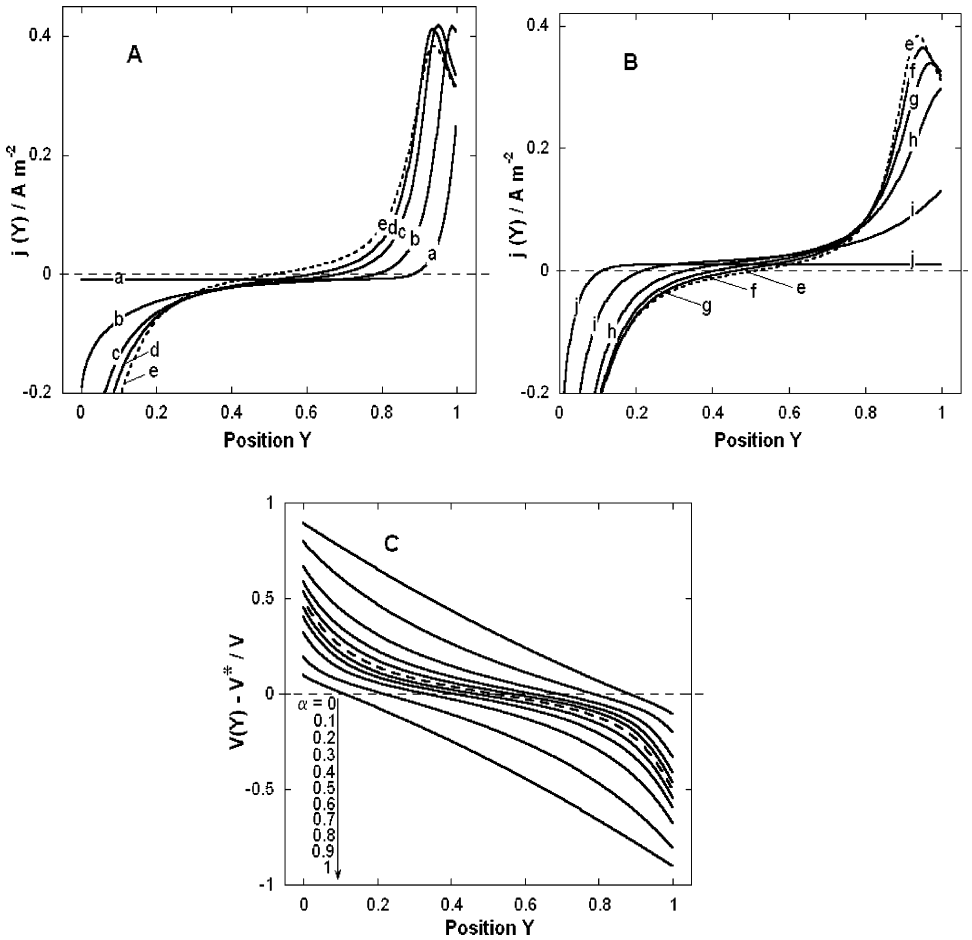

Figure 7. Spatial distributions of the local faradaic current density $j(Y)$ (panels A and B) and the local potential $V(Y)$ (panel C) along the conducting surface at different electron-transfer coefficients α. In (A) and (B), $\alpha = 0$ (a), 0.1 (b), 0.2 (c), 0.3 (d), 0.5 (e), 0.6 (f), 0.7 (g), 0.8 (h), 0.9 (i), and 1 (j). For the sake of readability, the curves corresponding to $\alpha = 0.5$ (symmetrical case) are indicated in dashed form. Model parameters: $k_o = 10^{-6}$ m s^{-1}, $\Delta\varphi_s = 1$ V, and $\Delta P = 1$ kPa, otherwise they are the same as those in Figure 2.

of Y_o on α is particularly clear when examining the profiles $V(Y) - V^*$ (Figure 7C). For $\alpha = 0$, the cathodic process spans over a large range of lateral positions Y with a quasi-linear distribution of potential (because of small local current densities). The maximum deviation from linearity is met for $\alpha = {}^1/_2$ where the bipolar current is the larger (within the condition $c^*_{Ox} = c^*_R$; see section 3.2.3). The set of eqs 12 and 19−21 is invariant upon the following transformations

$$\alpha \rightarrow 1 - \alpha \tag{24}$$

$$c_{Ox}(X = \pm 1, Y) \rightarrow c_R(X = \pm 1, Y) \tag{25}$$

and

$$V(Y) - V^* \rightarrow -\{V(Y) - V^*\} \tag{26}$$

This mathematical specificity explains why the profiles for the potential (Figure 7C) and surface concentrations (read from Figure 6) calculated for α and $1 - \alpha$ are antisymmetric around the position $Y_o(\alpha = {}^1/_2) \approx 0.5$ for $k_o = 10^{-6}$ m s^{-1}, as adopted in the calculations. This antisymmetry disappears when the value of $Y_o(\alpha = {}^1/_2)$, as fixed by the kinetic and the convective diffusion characteristics of the e.t. reaction, significantly differs from 0.5 (not shown). It is further noted that the invariance expressed by eqs 24−26 strictly applies for $c^*_{Ox}/c^*_R = 1$ (to ensure the equivalence between anodic and cathodic areas upon the permutation given by eq 25) and does not pertain to the current density profiles which are strongly modulated by the spatial distribution of the diffusion layer thickness along the electrode surface (see parts A and B of Figure 7).

3.2.3. Bipolar Current I_f. The variations of the bipolar current with the transfer coefficient α are given in Figure 8 for fixed electrohydrodynamic conditions $\Delta\varphi_s/\Delta P$ and various values of the rate constant k_o (panel A). For $k_o \gg 1$, the rate of the reversible reaction 1 is only a function of the mass-transport processes of the electroactive species to/from the surface, so that $\partial I_f/\partial\alpha = 0$. For finite values of k_o compatible with a quasi-reversible functioning of the bipolar processes, a dependence of I_f on α arises. I_f is maximum for $\alpha = {}^1/_2$ and decreases for $\alpha > {}^1/_2$ and $\alpha < {}^1/_2$ with $I_f(\alpha) \approx I_f(1 - \alpha)$ (panel A). The presence of this parabolic-like profile for I_f is a straightforward consequence of the (anti)symmetry properties of the potential distribution, discussed in section 3.2.2. When k_o is increased, this antisymmetry gradually disappears (because $Y_o(\alpha = {}^1/_2) \neq 0.5$; see Figure 5A), but in the meantime, the potential profiles are altered to a lesser extent by changes in α (approach of the reversible limit). As a result, only small deviations of the ratio $I_f(\alpha)/I_f(1 - \alpha)$ from 1 are encountered upon the increase of k_o.

When the ratio of c^*_{Ox}/c^*_R (Figure 8B) is changed for given electrode kinetic and convective diffusion conditions, the spatial distributions for the species concentrations, current density, and potential become increasingly asymmetric with significant departures of Y_o from the value 0.5. This asymmetry, which compounds the one due to the spatial distribution of the diffusion layer along the electrode surfaces, implies a loss of symmetry for I_f with respect to $\alpha = {}^1/_2$. In particular, the maximum in I_f

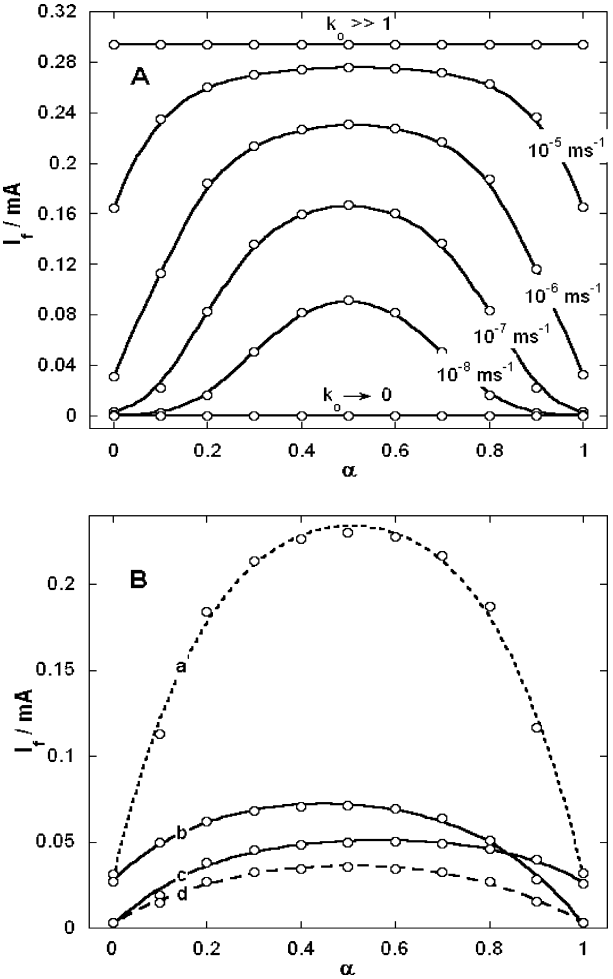

Figure 8. (A) Bipolar current (points) as a function of the electron-transfer coefficient α at different kinetic constant k_o (indicated). Other model parameters are the same as those in Figure 2 except $\Delta P = 1$ kPa and $\Delta\varphi_s = 1$ V. (B) Bipolar current (points) as a function of the electron-transfer coefficient α for various ratios of c^*_{Ox}/c^*_R: (a) $c^*_{Ox} = c^*_R = 0.1$ mM, (b) $c^*_{Ox} = 0.1$ mM $= 10c^*_R$, (c) $c^*_R = 0.1$ mM $= 10c^*_{Ox}$, and (d) $c^*_{Ox} = c^*_R = 0.01$ mM. The symmetrical cases (a) and (d) are indicated by the dashed lines. Other model parameters are the same as those in Figure 8A except $k_o = 10^{-6}$ m s^{-1}. The lines (plain and dashed) are only guides to the eye.

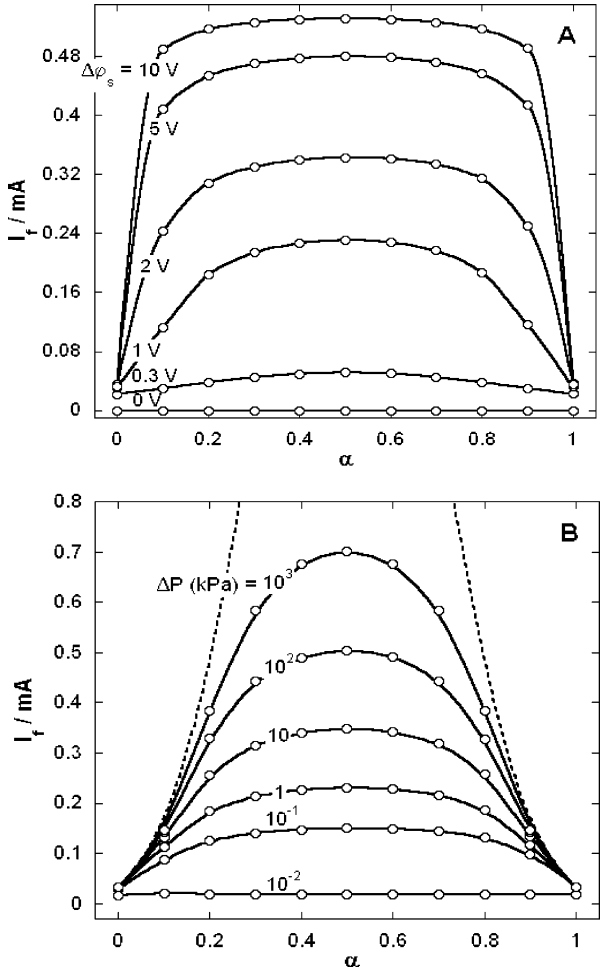

Figure 9. Bipolar current (points) as a function of the electron-transfer coefficient α at different electric fields $\Delta\varphi_s$ (A) and applied pressures ΔP (B). Model parameters are the same as those in Figure 2 with $k_o = 10^{-6}$ m s^{-1}, $\Delta P = 1$ kPa (A), and $\Delta\varphi_s = 1$ V (B). The lines are only guides to the eye. The dashed line in panel B represents the bipolar current as computed for irreversible—that is, kinetically controlled—anodic and cathodic reactions.

is shifted to lower α when increasing the ratio of c^*_{Ox}/c^*_R, which is in line with the impact of α on the concentration profiles as discussed in Figure 6.

Finally, Figure 9 shows the dependence of I_f on α for various applied fields $\Delta\varphi_s$ (Figure 9A) and pressure gradients ΔP (Figure 9B). Qualitatively, an increase of $\Delta\varphi_s$ for constant α results in an increase of I_f, as expected from analysis of Figure 2B (section 3.1.1). For sufficiently large values of $\Delta\varphi_s$ and $0 < \alpha < 1$, we have $\partial I_f/\partial\alpha \rightarrow 0$ because I_f approaches the diffusive limiting current I^l_f which is independent of the electrode kinetics. For $\alpha = 0$ and $\alpha = 1$, the quasi-reversible currents $I_f(\Delta\varphi_s \gg 1)$ tend to a constant value which is lower than I^l_f. This is so because the argument of the exponential function in the expression of either the cathodic or the anodic current (eq 12) cancels. This in turn limits the increase of I_f with increasing electric field strength. For given α and $\Delta\varphi_s$, I_f increases with ΔP (panel B) because of the concomitant decrease of the diffusion length for every position Y along the electrode. Since kinetic limitation of the bipolar processes is enhanced upon the increase of ΔP (section 3.1.1), the dependence of I_f on α becomes more and more pronounced with increasing values of ΔP. In the limit $\Delta P \rightarrow \infty$, I_f approaches the current for irreversible bipolar faradaic depolarization of the metal/electrolyte interface (dashed curve). The symmetry properties of I_f with respect to $\alpha = {}^1/_2$ (panels A and B) are in agreement with the discussion in the preceding sections.

3.3. Electrokinetic Properties of Metal Surfaces Depolarized by Quasi-reversible Bipolar Faradaic Processes. In the frame of electrokinetic experiments, a potential difference called the streaming potential and denoted as $\Delta\varphi_{str}$ is built up across the cell upon application of a pressure drop ΔP along the surface. When the solution contains electroactive species and the surfaces are conducting, sufficiently large $\Delta\varphi_{str}$ may induce a bipolar electrodic behavior of the surfaces in the same way as described in sections 3.1−3.2.[4] For such systems, derivation of the interfacial electrokinetic potential ζ from the raw $\Delta\varphi_{str}$ data on the basis of approaches that disregard bipolar depolarization, such as the linear Helmholtz−Smoluchowski (H−S) equation, is not possible.[4] Instead, the H−S formalism must be extended with the appropriate bipolar conduction term, to give[1]

$$\frac{\epsilon_0\epsilon_r\zeta\Delta P}{\eta} = -L_0K^L\left.\frac{\partial V(y,\Delta\varphi_{str},\Delta P)}{\partial y}\right|_{y=y_0} + \frac{L_0}{al}I_f(\Delta\varphi_{str},\Delta P) \quad (27)$$

where surface conduction is ignored. ϵ_o denotes the dielectric

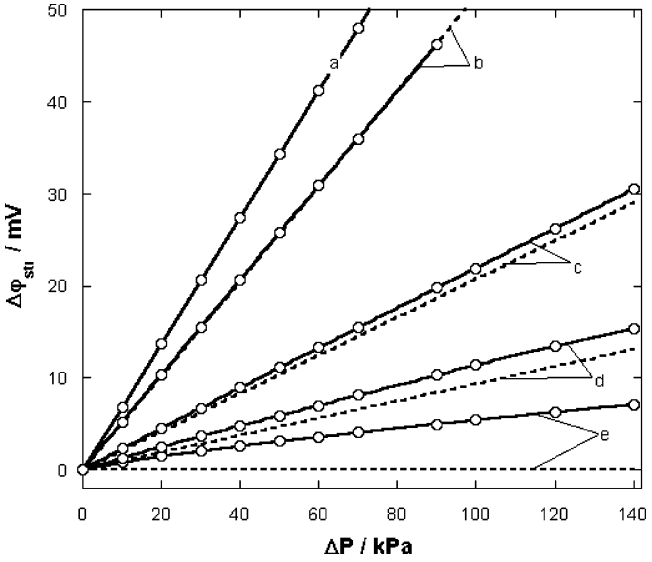

Figure 10. Reconstruction of the streaming potential $\Delta\varphi_{str}$−pressure ΔP plots (points) for a given ζ-potential, $\zeta = 100$ mV, and various electron-transfer rate constants: $k_o \rightarrow 0$ (a), $k_o = 10^{-6}$ (b), $k_o = 10^{-5}$ (c), $k_o = 5 \times 10^{-5}$ m s^{-1} (d), and $k_o \rightarrow \infty$ m s^{-1} (e). Parameters: $a =$ 1 mm, $L_0 = 7.6$ cm, $l = 2.6$ cm, $D = 5 \times 10^{-10}$ m^2 s^{-1}, $V^0 = -233$ mV, $K^L = 0.1\ \Omega^{-1}$ m^{-1}, and $c^*_{Ox} = c^*_R = 10^{-5}$ M. Curve (a) coincides with that calculated on the basis of the linear Helmholtz−Smoluchowski equation whereas the (plain) curve (e) pertains to the fully reversible bipolar faradaic depolarization of the double layer (reversible electron-transfer reactions). The dashed lines are computed with the approximate expression given in eq 28, which neglects concentration polarization (irreversible electron-transfer reactions). The plain lines are only guides to the eye.

permittivity of vacuum. For $I_f \rightarrow 0$, the potential distribution is linear and eq 27 reduces to the classical H−S equation. The impact of the electronic conduction term (second term in the right-hand side of eq 27) was analyzed in ref 1 where fully reversible bipolar processes were considered. Here, we expand the analysis by taking into account the kinetic limitation of the e.t. reaction which is a function of position along the metallic surface (sections 3.1.2 and 3.1.3). It is emphasized that, for *any finite* value of the intrinsic rate constant k_o, the coupled spatial distribution of the concentration polarization and overpotentials will *always* result in some kinetic limitation for the e.t., the rate of which is more or less critical depending on the electrohydrodynamic conditions (section 3.1.1) and lateral position (sections 3.1.2−3.1.3). In the previous sections, an electric field was applied in the solution along the surfaces and was, for practical reasons, set to be independent of the concomitantly operating pressure gradient. Within the framework of electrokinetics, these two quantities are coupled, as expressed by eq 27. Under steady-state conditions, the bipolar current generated by the streaming potential $\Delta\varphi_{str}$ as resulting from the pressure ΔP is the same as that obtained by externally applying the same pressure gradient and a potential difference $\Delta\varphi_s = \Delta\varphi_{str}$.

In Figure 10, reconstruction of the $\Delta\varphi_{str}-\Delta P$ plots is given for $\zeta = 100$ mV and various values of the rate constant k_o, with the other parameters being constant. It is noted that the pressure range covered by Figure 10 corresponds to common practice.[4,8] Graphical interpretation of the computational procedure followed for the determination of the $\Delta\varphi_{str}-\Delta P$ plots is extensively discussed in ref 1. In the limit $k_o \rightarrow 0$, the faradaic contribution I_f to the total back-current is very low as compared with that originating from ionic conduction so that linearity between $\Delta\varphi_{str}$ and ΔP, as predicted by the H−S equation, is recovered. When $k_o$is increased, I_f increases in parallel and the $\Delta\varphi_{str}-\Delta P$ curves develop a bend. The resulting deviations from linearity are dictated by the nonlinear dependence of the bipolar current I_f on $\Delta\varphi_{str}$, ΔP, and k_o (Figure 2). The larger the k_o values, the larger the back electronic conduction and the more significant the suppression of the streaming potential at a given pressure. For $k_o \rightarrow \infty$, the reversible limit is reached.[1]

As discussed in section 3.1, the kinetic limitation of the e.t. Reaction 1 increases notably with the pressure ΔP. In ref 8, an approximate analytical expression for the streaming-potential was derived for the case where the local current densities are limited by the interfacial e.t. kinetics only. The result reads as

$$\Delta\varphi_{str} = \frac{2\epsilon_0\epsilon_r\zeta\Delta P}{\eta L_0 K^L \omega \coth(\omega L_0/2)} \qquad (28)$$

with $\omega = F\{k_o(c^*_{Ox} + c^*_R)/RTaK^L\}^{1/2}$. Equation 28 is the limit of eq 27 for $c_{Ox,R}(X = \pm 1, Y) = c^*_{Ox,R}$ and is valid for relatively small overpotentials $V(Y) - V^*$ (so that linearization of eq 12 is possible[8]), which is consistent with the measured streaming potential values $\Delta\varphi_{str}$ typically reported in the literature. In Figure 10, the $\Delta\varphi_{str}-\Delta P$ curves as derived from eq 28 are shown. As expected, agreement with numerical results is excellent for sufficiently low values of k_o, where mass-transport does not critically govern the rate of reaction 1. Upon increase of k_o, deviations appear which increase with increasing pressure. Obviously, for $k_o \rightarrow \infty$, eq 28 is totally inadequate since reversibility applies. Careful inspection of the curves obtained from the rigorous treatment of the electrokinetics for quasi-reversible bipolar depolarization (curves c and d) reveal that for large ΔP the slope $\Delta\varphi_{str}/\Delta P$ approaches that inferred from eq 28. This corroborates the analysis above on the dependence of the degree of reversibility with hydrodynamics. The origin of the linear regime as observed for $k_o \rightarrow \infty$ (curve e) and sufficiently large ΔP is fundamentally different and has been discussed in sufficient detail in ref 1.

As a final remark, derivation of the electrokinetic potential ζ from given streaming potential data can be performed by exploiting the high-pressure regime and eq 28, providing that the redox processes are sufficiently limited by electrode kinetics. This was done in ref 8 for the interpretation of streaming potentials measured on (bipolar) gold electrodes in the presence of the redox couple $Fe(CN)_6^{3-}/Fe(CN)_6^{4-}$. The evidence for the high degree of irreversibility of that couple on gold under the experimental conditions of ref 8 was found after a critical quantitative analysis of monopolar voltammetric data.

4. Conclusions

The bipolar behavior of metallic surfaces in a thin-layer cell of the type used for electrokinetic experiments is described in the most general situation where the extent of faradaic depolarization is controlled by convective diffusion of the electroactive species to/from the surface and by the kinetics of the interfacial electron transfer (quasi-reversibility). A detailed analysis of the resulting bipolar faradaic current and spatial distributions of overpotentials, species concentrations, and local current densities is presented. It is based on a numerical integration procedure for the complex coupling of the Nernst−Planck equation with the Poisson equation for finite currents. The latter are defined by the Butler−Volmer equation extended with the appropriate mass-transfer expressions. The limiting cases of totally irreversible or totally reversible e.t. reactions, as studied in previous analyses,[1,5] are very well reproduced.

The subtle interplay between electrodic, electric, and hydrodynamic variables results in a position-dependent degree of reversiblity for the e.t. along the surface. Typically, reversibility increases downstream with increasing concentration polarization in the direction given by the hydrodynamic flow. Similar to monopolar reactions, the degree of reversibility is also dependent on the electrohydrodynamic conditions. Strong electric fields largely overrule e.t. polarization, whereas strong pressure gradients reduce concentration polarization. The variation of reversibility with position considerably alters the (as)symmetry of the species concentration distribution along the surface. The impact of the electrode kinetics on the symmetry properties of the bipolar faradaic process comes on top of that induced by the spatial profile of the diffusion layer as resulting from the imposed lateral hydrodynamic field.

The consequences for the electrokinetic properties of metallic surfaces in the presence of a quasi-reversible redox couple are analyzed. In particular, it is shown how the deviations of the streaming potential−pressure plots from linearity as a result of electronic back-conduction are coupled to the dependence of the bipolar current on the electrode kinetics. The corresponding formalism completes the rigorous basis for a quantitative interpretation of electrokinetic features of electron conducting surfaces depolarized by either irreversible, quasi-reversible, or reversible bipolar faradaic processes.

Glossary

a	Gap of the thin-layer chamber
c_{Ox}	Local concentration of the Ox species
c^*_{Ox}	Bulk concentration of the Ox species
c_R	Local concentration of the R species
c^*_R	Bulk concentration of the R species
C_{Ox}	Dimensionless concentration difference for the Ox species
C_R	Dimensionless concentration difference for the R species
D_{Ox}	Diffusion coefficient for the Ox species
D_R	Diffusion coefficient for the R species
D	Diffusion coefficient $D = D_{Ox} = D_R$
f	Defined by F/RT
F	Faraday number
$G(Y)$	Function of the position given by eq 17
I_f	Overall bipolar current
j	Local current density
K^L	Conductivity of the electrolyte solution
k_o	Rate constant of the electron-transfer reaction 1
l	Width of the metallic substrates
l	As superscript pertaining to the diffusion limiting-current condition noted I^l_f
L_0	Length of the metallic substrates
n	Number of electrons
Ox	Oxidized species
$Q(Y)$	Function of the position given by eq 16
R	Reduced species
R	Gas constant
T	Temperature
v_Y	Velocity flow according to the Y-axis in the thin-layer channel
v^0	Characteristic velocity of the solution in the thin-layer channel
V	Local potential of the solution with respect to the equipotential metallic phase
V^0	Minus the standard potential for the redox couple Ox/R
V^*	Potential at $Y = Y_0$
x,y,z	Cartesian coordinates
X,Y,Z	Dimensionless Cartesian coordinates
Y_0	Position for which $j(Y = Y_0) = 0$
α	Transfer coefficient associated with the electron-transfer reaction 1
β	Ratio defined by $\beta = (c_{Ox}/c_R)_{X=1,k_o}/(c_{Ox}/c_R)_{X=1,ko\to\infty}$ (see Figure 4G)
$\Delta\varphi_s$	Lateral applied potential difference
$\Delta\varphi_{str}$	Streaming potential
ΔP	Tangential applied pressure drop
δ	Thickness of the diffusion layer
ϵ_0	Dielectric permittivity of vacuum
ϵ_r	Relative dielectric permittivity of water
ϕ	Ratio a/l
κ	Inverse of the Debye length
η	Dynamic viscosity
τ_M	Characteristic time at which the streaming potential measurements are performed
ζ	Electrokinetic potential (ζ-potential)

Appendix

Computation of the Concentration Profiles $c_{Ox}(X,Y)$, the Spatial Distributions of the Potential $V(Y)$, and the Local Faradaic Current Density $j(Y)$. Contrary to the study made of the transient characteristics for diffusion-limited bipolar processes,[5] decoupling of the transport eq 8 and the Poisson eq 19 in the current problem cannot be simply performed by analytical means. Therefore, as for the analysis of reversible faradaic depolarization in the electrokinetics of conducting surfaces,[1] a consistent numerical solution of the complete set of eqs 8, 9, 12, 14−17, and 19−21 must be found.

Discretization of the Convective Diffusion Equation. The problem is symmetrical with respect to $X = 0$, so that in the following the analysis will be restricted to the interval $0 \le X \le 1$. By the use of this symmetry argument, the boundary conditions associated with eq 8 in the text are

$$C_{Ox}(X = +1,Y) = Q(Y) - \gamma j(Y)G(Y) \qquad \text{(A1)}$$

$$\frac{\partial C_{Ox}(X,Y)}{\partial X}\Big|_{X=0} = 0 \qquad \text{(A2)}$$

where γ, $Q(Y)$, and $G(Y)$ are given by eqs 15, 16, and 17, respectively. The local faradaic current density $j(Y)$ is defined by

$$j(Y) = \sigma \frac{\partial C_{Ox}(X,Y)}{\partial X}\Big|_{X=1} \qquad \text{(A3)}$$

with $\sigma = 2nFDc^*_{ox}/a$. The spatial variables X and Y are written

$$i \in [1,M]: \quad X_i = (i-1)\Delta X \qquad \text{(A4)}$$

$$k \in [1,N]: \quad Y_k = (k-1)\Delta Y \qquad \text{(A5)}$$

where M and N are integers and ΔX and ΔY the spatial steps for the X and Y directions, respectively. For the sake of simplicity, we write $C_{Ox}(X_i,Y_k) = C_{i,k}$, $Q(Y_k) = Q_k$, $G(Y_k) = G_k$, and $j(Y_k) = j_k$. To optimize the convergence of the iteration scheme described below, the inverse-Euler method[14] was chosen

for discretizing eqs 8, A2, and A3. For a given position Y_k, one obtains

$i \in [2,M-1]$:

$$-r_i C_{i-1,k-1} + (1+2r_i)C_{i,k+1} - r_i C_{i-1,k+1} = C_{i,k} \quad \text{(A6)}$$

$$C_{1,k+1} - C_{2,k+1} = 0 \quad \text{(A7)}$$

$$\frac{\sigma}{\Delta X}(C_{M,k+1} - C_{M-1,k+1}) = j_{k+1} \quad \text{(A8)}$$

with r_i the quantity defined by

$i \in [2,M-1]$:

$$r_i = \frac{4DL_0}{v^0 a^2}\frac{\Delta Y}{[1-(i-1)^2\Delta X^2]\Delta X^2} \quad \text{(A9)}$$

Equations A6−A8 can be written for every k in the matricial form

$$k \in [1,N]: \quad T\cdot\vec{C}_{k+1} = \vec{C}_k \quad \text{(A10)}$$

with $\vec{C}_{k+1}$ and $\vec{C}_k$ the column vectors

$$\vec{C}_{k+1} = \begin{pmatrix} C_{1,k+1} \\ C_{2,k+1} \\ C_{3,k+1} \\ \vdots \\ \vdots \\ C_{M,k+1} \end{pmatrix} \quad \vec{C}_k = \begin{pmatrix} 0 \\ C_{2,k} \\ C_{3,k} \\ \vdots \\ C_{M-1,k} \\ j_{k+1} \end{pmatrix} \quad \text{(A11)}$$

and T the tridiagonal matrix of dimension $M \times M$

$$T = \begin{pmatrix} 1 & -1 & 0 & \cdots & \cdots & \cdots & 0 \\ -r_2 & 1+2r_2 & -r_2 & \ddots & & & \vdots \\ 0 & -r_3 & 1+2r_3 & -r_3 & 0 & & \vdots \\ \vdots & \ddots & & & & \ddots & \vdots \\ \vdots & & 0 & & & & 0 \\ \vdots & & & \ddots & -r_{M-1} & 1+2r_{M-1} & -r_{M-1} \\ 0 & \cdots & \cdots & \cdots & 0 & -\sigma/\Delta X & \sigma/\Delta X \end{pmatrix} \quad \text{(A12)}$$

To solve eq A10 for every k, the values of the components $(j_k)_{k\in[1,N]}$ of the column vector $\vec{j}$ are required. The $(j_k)_{k\in[1,N]}$ depends on the potential distribution $\{V(Y_k)\}_{k\in[1,N]} = (V_k)_{k\in[1,N]}$ and the surface concentrations C_{Ox} $(X=1, Y_k) = (C_{M,k})_{k\in[1,N]}$, as formulated by eqs 12 and 14−17. Because the M^2 elements of the matrix T are independent of k, one may easily show that the local current density j_k is, for every position k along the bipolar electrode, linearly related to the concentrations $C_{i,k}$. Particularly, one infers the existence of a linear relationship between the j_k and the corresponding surface concentration $C_{M,k}$. Denoting $\vec{C}_S$ the column vector of components $(C_{M,k})_{k\in[1,N]}$, we conclude that there is a matrix A of dimension $N \times N$ such that

$$\vec{C}_S = A\cdot\vec{j} \quad \text{(A13)}$$

The vectorial relation (eq A13) allows the decoupling of the transport and electric problems, as we shall demonstrate in the following.

Calculation of the Matrix A. Let $\mathcal{T}$ be a numerical solver which enables the calculation of the searched $\vec{C}_k$ from a known solution $\vec{C}_{k-1}$ and a given vector $\vec{j}$

$$k \in [1,N]: \quad \vec{C}_k = \mathcal{T}(\vec{C}_{k-1}, \vec{j}) \quad \text{(A14)}$$

Iterating k from 1 to N, with $\vec{C}_0 = \vec{0}$ as a starting solution, the $(C_{i,k})_{i\in[1,M],k\in[1,N]}$, and in particular the $(C_{M,k})_{k\in[1,N]}$, can be obtained. The numerical method subsumed in $\mathcal{T}$ for solving the linear algebraic tridiagonal system (eq A10) is based on a simple form taken by the classical Gaussian elimination technique with partial pivoting.[15] Let us consider N sets of solutions $(\vec{C}_k^{*(n)})_{n\in[1,N]}$ verifying

$$n \in [1,N]: \quad C_k^{*(n)} = \mathcal{T}(\vec{C}_{k-1}^{*(n)}, \vec{e}_n) \quad \text{(A15)}$$

where $\vec{e}_n$ are the vectors of the canonical base of dimension N

$$\vec{e}_n = \begin{pmatrix} 0 \\ \vdots \\ 1 \\ 0 \\ \vdots \\ 0 \end{pmatrix} \leftarrow n\text{th position} \quad \text{(A16)}$$

The asterix denotes that the solutions $(\vec{C}_k^{*(n)})_{n\in[1,N]}$ considered at this stage of the analysis are not physically relevant: they are only used for the algebraic determination of the matrix A. The corresponding vector containing the surface concentrations $(\vec{C}_{M,k}^{*(n)})_{n\in[1,N],k\in[1,N]}$ is denoted $(\vec{C}_S^{*(n)})_{n\in[1,N]}$. For every n, using eq A13, we have the matricial relations

$$n \in [1,N]: \quad \vec{C}_S^{*(n)} = A\cdot\vec{e}_n \quad \text{(A17)}$$

Because of the choice made for the $\vec{e}_n$, the vector $\vec{C}_S^{*(n)}$ actually represents the nth column of matrix A. One can further show that the components of the vector $\vec{C}_S^{*(n)}$ are simply shifted with respect to those of the vector $\vec{C}_S^{*(n-1)}$ so that computation of eq A15 for $n = 1$ suffices to generate all the elements of A. Consequently, A has the particular following tridiagonal form

$$A = \begin{pmatrix} C_{M,1}^{*(1)} & 0 & 0 & \cdots & 0 \\ C_{M,2}^{*(1)} & C_{M,1}^{*(1)} & 0 & & 0 \\ C_{M,3}^{*(1)} & C_{M,2}^{*(1)} & C_{M,1}^{*(1)} & \ddots & \vdots \\ \vdots & \vdots & \vdots & \ddots & 0 \\ C_{M,N}^{*(1)} & C_{M,N-1}^{*(1)} & C_{M,N-2}^{*(1)} & \cdots & C_{M,1}^{*(1)} \end{pmatrix} \quad \text{(A18)}$$

Discretization of the Poisson Equation and the Boundary Condition (eq A1): Computation of the Potential and Current Density Distributions. Discretization of eqs 14 and 19−21 leads to

$k \in [2,N-1]$:

$$V_{k-1} - 2V_k + V_{k+1} + \mu j_k = 0 \quad \text{(A19)}$$

$$-V_1 + V_2 + V_{N-1} + V_N = 0 \quad \text{(A20)}$$

$$V_1 - V_N - \Delta\varphi_s = 0 \quad \text{(A21)}$$

$k \in [1,N]$:

$$C_{M,k} - Q_k + \gamma j_k G_k = 0 \quad \text{(A22)}$$

with μ the constant given by

$$\mu = \frac{2L_0\Delta Y^2}{aK^L} \quad \text{(A23)}$$

Through the use of the relationship A13, eq A22 may be rewritten in the form

$$k \in [1,N]: \quad \sum_{p=1}^{N} a_{k,p} j_p - Q_k + \gamma j_k G_k = 0 \quad \text{(A24)}$$

with $(a_{k,p})_{k\in[1,N],p\in[1,N]}$ the components of matrix A as determined in the previous section (eq A18). Q_k and G_k are functions of V_k defined by

$$Q_k = \frac{c_{Ox}^* + c_R^*}{c_{Ox}^*} \frac{\exp[-nf(V_k - V^0)]}{1 + \exp[-nf(V_k - V^0)]} - 1 \quad \text{(A25)}$$

and

$$G_k = \frac{\exp[-\alpha nf(V_k - V^0)]}{1 + \exp[-nf(V_k - V^0)]} \quad \text{(A26)}$$

respectively. The nonlinear system consisting of the $2N$ equations A19−A21 and A24 has the potentials V_k and j_k as the only unknown variables. This system was solved using a Newton−Raphson type method.[15] Once the j_k values are known, the local concentration profiles $\vec{C}_k$ are then calculated using eq A14. The ensuing bipolar current I_f was obtained by integrating the local faradaic currents by means of the trapezoid method.

Errors Inherent to the Discrete Analysis of the Problem. The error made using the inverse Euler method applied to the convective diffusion equation (eqs A6−A8) is of the order $O(\Delta Y + \Delta X^2)$, and the one made in the finite difference scheme applied to the local electroneutrality equation (eqs A19−A21) is $O(\Delta Y^2)$.[14,16] The computations were made with $M = 10^4$ iterations for the X direction and $N = 500-10^3$ iterations for the Y direction, which yields convergence of the results within a satisfactory computation time.

The numerical scheme adopted in the problem analyzed here is largely inspired from that used for reversible bipolar processes.[1] The notable difference is that the significant nonlinear coupling between the transport and Poisson equation, as subsumed in eq A1, *imposes* to reason in terms of a vectorial relationship between $\vec{C}_S$ and $\vec{j}$ (eq A13) and *not* between $\vec{j}$ and $\vec{Q}$ (vector of elements $(Q_k)_{k\in[1,N]}$), as done in ref 1.

References and Notes

(1) Duval, J.; van Leeuwen, H. P.; Cecilia, J.; Galceran, J. *J. Phys. Chem. B* **2003**, *107*, 6782.

(2) Van Wagenen, R. A.; Andrade, J. D. *J. Colloid Interface Sci.* **1980**, *76 (2)*, 305.

(3) Scales, P. J.; Grieser, F.; Healy, T. W.; White, L. R.; Chan, D. Y. C. *Langmuir* **1992**, *8*, 965.

(4) Duval, J.; Huijs, G. K.; Threels, W. F.; Lyklema, J.; van Leeuwen, H. P. *J. Colloid Interface Sci.* **2003**, *260*, 95.

(5) Duval, J.; Minor, M.; Cecilia, J.; van Leeuwen, H. P. *J. Phys. Chem. B* **2003**, *107*, 4143.

(6) Bard, A. J.; Faulkner, L. R. *Electrochemical Methods Fundamentals and Applications*; John Wiley and Sons: New York, 1980; Chapter 3, p 86.

(7) White, F. M. *Fluid Mechanics*, 2nd ed.; McGraw-Hill: New York, 1986.

(8) Duval, J. *J. Colloid Interface Sci.* **2004**, 269 (1), 211.

(9) Conway, B. E. *Theory and Principles of Electrode Processes*; Ronald: New York, 1965; Chapters 4 and 5.

(10) Bard, A. J.; Faulkner, L. R. *Electrochemical Methods Fundamentals and Applications*; John Wiley and Sons: 1980; Chapter 3, p 96 and references therein.

(11) Levich, V. G. *Physicochemical Hydrodynamics*; Prentice-Hall: Englewood Cliffs, NJ, 1962.

(12) Duval, J.; Kleijn, J. M.; van Leeuwen, H. P. *J. Electroanal. Chem.* **2001**, *505*, 1.

(13) Bard, A. J.; Faulkner, L. R. *Electrochemical Methods Fundamentals and Applications*; John Wiley and Sons: 1980; Chapter 3, p 94 and references therein.

(14) Ames, W. F. *Numerical Methods for Partial Differential Equations*, 3rd ed.; Academic Press: Boston, MA, 1992.

(15) Press, W. H.; Teukolsky, S. A.; Vetterling, W. T.; Flannery, B. P. *Numerical Recipes in Fortran, The Art of Scientific Computing*, 2nd ed.; Cambridge University Press: Cambridge, U.K., 1986.

(16) Dautray, R.; Lions, J. L. *Analyse Mathématique et Calcul Numérique pour les Sciences et les Techniques, Evolution Numérique, Transport*; Masson: Paris, 1988; Vol. 9.